

# Understanding current-driven dynamics of magnetic domain walls in systems with spin-orbit coupling

Mei Li<sup>1,2</sup>, Jianbo Wang<sup>2,4</sup> and Jie Lu<sup>3,4</sup>

<sup>1</sup> Physics Department, Shijiazhuang University, Shijiazhuang, Hebei 050035, China

<sup>2</sup> School of Physics and Technology, Center for Electron Microscopy and MOE Key Laboratory of Artificial Micro- and Nano-structures, Wuhan University, Wuhan 430072, China

<sup>3</sup> College of Physics and Information Engineering, Hebei Advanced Thin Films Laboratory, Hebei Normal University, Shijiazhuang 050024, China

<sup>4</sup> Authors to whom any correspondence should be addressed.

E-mail: wang@whu.edu.cn, jlu@hebtu.edu.cn

**Abstract.** In this work, systematic one-dimensional (1D) analyses are performed to provide analytical understandings on current-driven domain-wall dynamics in heavy metal/ferromagnetic metal/oxide trilayers. When spin-orbit torques (SOTs) induced by Rashba spin-orbit interaction or spin Hall effect are considered, in 1D collective-coordinate-model framework the Walker breakdown suppression is explained in the presence of fieldlike (FL) SOTs with effective fields along  $\mathbf{e}_z \times \hat{\mathbf{J}}_e$  ( $\mathbf{e}_z$  being the interface normal and  $\hat{\mathbf{J}}_e$  being the charge current direction). While the wall mobility (velocity versus current density) change and even motion-direction reversal (from forward to backward of electron flow) as well as its polarity sensitivity can be well explicated only if the anti-damping-like (ADL) SOT is introduced. When FL-SOTs induced by bulk inversion asymmetry or strain with effective fields along general transverse orientation are further considered, asymptotic expansions on dynamical equation reveal that the mobility change still can not happen without the help of ADL-SOTs. This also holds for external uniform transverse magnetic fields with general orientations.

*Keywords:* spin-orbit coupling, spin-orbit torque, magnetic domain walls, current-driven dynamics, 1D collective coordinate model

Submitted to: *New J. Phys.*

## 1. Introduction

Pure current-induced domain wall (DW) propagation in magnetic nanostructures has attracted intensive attention for decades starting from academic interests in understanding the interplay between itinerant spinful electrons and localized magnetic moments[1, 2, 3, 4]. In monolayer ferromagnetic nanostrips, in-plane currents drive DWs to propagate along the direction of electron flow through the spin transfer process[5, 6, 7, 8, 9, 10, 11, 12, 13, 14, 15], which leads to promising applications in future magnetic racetrack memories[16, 17], shift registers[18, 19] and memristors[20, 21], etc. However, in these monolayers the wall velocity is at most  $10^2$  m/s even when the current density is up to  $10^8$  A/cm<sup>2</sup>. This comes from the fact that spin transfer torques (STTs) therein can not be strong as the exchange energy avoids abrupt changes in magnetization texture. To improve the current efficiency, the current-perpendicular-to-plane (CPP) configuration in narrow and long spin valves is proposed [22, 23, 24]: to reach the same velocity level ( $10^2$  m/s), the current density for “planar polarizer” case is reduced to  $10^7$  A/cm<sup>2</sup> while that for “perpendicular polarizer” can even be lowered to  $10^6$  A/cm<sup>2</sup>. However, the rapidly increasing CPP cross-section area largely offsets the decrease in current density. Even if the current is forced to focus on wall region, precise dynamical synchronization in real experiments remains challenging.

Over the past decade, in heavy metal/ferromagnetic metal/oxide (HM/FMM/Oxide) trilayers, axial DW propagation in FMM layer with perpendicular magnetic anisotropy (PMA) driven by in-plane currents are experimentally observed[25, 26, 27, 28, 29, 30, 31, 32, 33, 34, 35, 36, 37, 38, 39, 40, 41]. In certain case, walls can move at a high velocity up to 400 m/s when current density is around  $10^8$  A/cm<sup>2</sup>[37]. More interestingly, DWs with certain polarity can even move in the direction of charge current[33, 34, 35, 36, 37, 38, 39, 40, 41], which is also confirmed by numerical simulations [42, 43, 44, 45]. To understand these findings, spin-orbit torques (SOTs) from strong spin-orbit coupling (SOC) in these trilayers are proposed [46, 47, 48, 49, 50, 51, 52, 53, 54, 55, 56, 57, 58, 59]. Suppose  $\hat{\mathbf{J}}_e$  is the charge current direction and  $\mathbf{e}_z$  is interface normal. Mathematically, SOTs can be decomposed into two perpendicular components: (a)  $\propto \mathbf{m} \times (\hat{\mathbf{J}}_e \times \mathbf{e}_z)$  which is odd in magnetization direction  $\mathbf{m}$  and usually referred to as fieldlike (FL) torque; (b)  $\propto \mathbf{m} \times [\mathbf{m} \times (\hat{\mathbf{J}}_e \times \mathbf{e}_z)]$  which is even in  $\mathbf{m}$  and usually called anti-damping-like (ADL) torque. Physically, two typical mechanisms are of most importance: the “spin Hall torques” from the spin Hall effect (SHE)[60] in HM layer and the “Rashba torques” from the structure inversion asymmetry (SIA) at the HM/FMM interface. In early literatures, ADL-SOTs are believed to stem mostly from bulk SHE while FL-SOTs are mainly attributed to interfacial Rashba SOC. However, recent works based on scattering-related mechanisms[52, 53, 54, 55, 56] and intrinsic Berry curvature[57, 58] reveal that Rashba SOC can cause FL and ADL SOTs with similar strength. Also, quantum tunneling of spin current from HMs to FMMs[59] allows SHE to provide FL and ADL SOTs with comparable magnitude. So far, physical source of SOTs is still a hot issue under debate[61, 62, 63, 64].

Meantime, analytics with Lagrangian functional[65, 66, 67] and simulations[68, 69, 70, 71, 72, 73, 74] based on Landau-Lifshitz-Gilbert (LLG) dynamical equation[75] have been performed to explain DW dynamics in HM/FMM/Oxide trilayers in the framework of one-dimensional collective coordinate model (1D-CCM). All these works focus on two novel features in experiments: (i) Walker breakdown (WB) suppression thus high wall velocity and (ii) DW motion opposed to electron flow and the corresponding “chirality sensitivity”. Historically, the Rashba-SOC-induced FL-SOT is first proposed to explain both novelties (i) and (ii)[68, 69, 70]. In addition, the novelty (ii) is also reproduced by only ADL-SOTs from SHE[71]. However, to our knowledge there are no explicit analytical expressions for WB suppression, the condition for DW motion reversal and the corresponding “chirality selection rule”. Explorations to these issues constitute the first part of this paper. On the other hand, in real trilayers SOC induced by bulk inversion asymmetry (BIA) or strain can also lead to FL-SOTs on magnetization texture with effective field along general transverse orientation other than  $\mathbf{e}_z \times \hat{\mathbf{J}}_e$ [76]. Moreover, torques from external uniform transverse magnetic fields (TMFs) share the same structure with these FL-SOTs. Systematic exploration of DW dynamics under these torques is another important issue and constitutes the second part of this article.

The rest of this paper is organized as follows. In section 2 the model and preparations are briefly introduced. Then in section 3 within 1D-CCM we provide analytical explanations to novelties (i) and (ii) when SIA or SHE-induced SOTs are involved. In section 4, modulations on DW dynamics by FL-SOTs from BIA, strain or torques from uniform TMFs are systematically investigated with the help of asymptotic expansion approach[77, 78, 79, 80] on LLG equation. Finally, the concluding remarks are provided in the last section.

## 2. Modeling and preparations

We consider a HM/FMM/Oxide trilayer with a DW formed in FMM layer. Generally, FMM layer has strong PMA or in-plane magnetic anisotropy (IPMA). Typical example for the former (latter) case is Co (NiFe). Meanwhile, the HM layer is composed of Pt or Ta in most experiments. For PMA systems, the coordinate system is depicted in figure 1a:  $\mathbf{e}_x$  shares the same direction with strip axis in which charge current density  $\mathbf{J}_e = J_e \mathbf{e}_x$  flows,  $\mathbf{e}_z$  is the interface normal and  $\mathbf{e}_y = \mathbf{e}_z \times \mathbf{e}_x$ . The easy (hard) axis of the FMM layer with PMA lies in  $\mathbf{e}_z$  ( $\mathbf{e}_x$ ) direction. As a result, the DW in it prefers to be a Bloch wall. After performing a unitary transformation  $\mathcal{U}_y(\pi/2)$  ( $\pi/2$  rotation around  $y$ -axis) on coordinates and magnetization texture (meanwhile leaving the trilayer and charge current density unchanged, see Ref. [42]), PMA systems in figure 1a can be converted to IPMA counterparts in figure 1b, with the Bloch wall turning to a Néel wall correspondingly. In the rest of this work we present our main results in the framework of PMA. Unless otherwise stated, most of the conclusions hold true for IPMA systems as well.

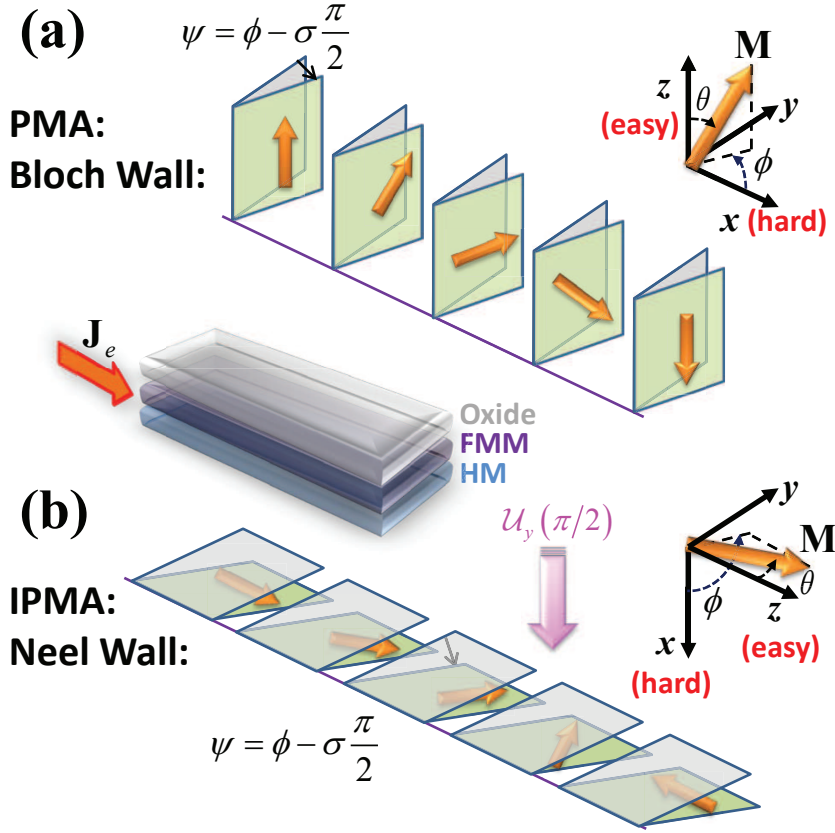


**Figure 1.** (Color online) Sketch of a typical HM/FMM/Oxide trilayer in which a Bloch (Néel) DW is formed in FMM layer with PMA (IPMA) as a result of energy minimization. The corresponding coordinate system is depicted at the upright corner in each subfigure. In fact, these two cases are connected by a unitary transformation  $\mathcal{U}_y(\pi/2)$  ( $\pi/2$  rotation around  $y$ -axis, pink arrow) performed on coordinates and magnetization texture. In each case, gray planes describe the planar  $\phi$ -distribution of static magnetization texture. When in-plane charge current  $\mathbf{J}_e$  is applied, magnetization vectors will be driven to tilt from their static locations by  $\psi$ , as indicated by the green planes. This sketch is inspired by figure 1 in Ref. [65].

### 2.1. Dynamical equation

In thin enough strips, most of the nonlocal magnetostatic energy can be described by local quadratic terms of  $M_{x,y,z}$  by means of three average demagnetization factors[79]. Thus in 1D-CCM, the total magnetic energy density functional takes the following explicit form,

$$\mathcal{E}[\mathbf{M}] = J(\nabla \mathbf{m})^2 - \frac{1}{2}k_E\mu_0 M_z^2 + \frac{1}{2}k_H\mu_0 M_x^2, \quad (1)$$

in which  $J(>0)$  is the exchange stiffness,  $k_E(k_H)$  is the total anisotropy coefficient along the easy (hard) axis. The time evolution of magnetization texture  $\mathbf{M}(\mathbf{r}, t) \equiv M_s \mathbf{m}(\mathbf{r}, t)$  with constant saturation magnetization  $M_s$  is governed by the generalized LLG equation,

$$\frac{\partial \mathbf{m}}{\partial t} = -\gamma \mathbf{m} \times \mathbf{H}_{\text{eff}} + \alpha \left( \mathbf{m} \times \frac{\partial \mathbf{m}}{\partial t} \right) + \mathbf{T}_{\text{SST}} + \mathbf{T}_{\text{SOT}}, \quad (2)$$

where  $\mathbf{H}_{\text{eff}} = -(\delta\mathcal{E}[\mathbf{M}]/\delta\mathbf{m})/(\mu_0 M_s)$  is the effective field,  $\gamma$  and  $\alpha$  are the gyromagnetic ratio and phenomenological damping coefficient, respectively. As passing through the trilayer, the charge current density is split into two parts:  $\mathbf{J}_e(t_F + t_H) = \mathbf{J}_e^F t_F + \mathbf{J}_e^H t_H$  with  $\mathbf{J}_e^F$  ( $\mathbf{J}_e^H$ ) being the component in FMM (HM) layer. From a simple circuit model[71], we have  $J_e^F = J_e(t_F + t_H)\sigma_F/(t_F\sigma_F + t_H\sigma_H)$  and  $J_e^H = J_e(t_F + t_H)\sigma_H/(t_F\sigma_F + t_H\sigma_H)$ , where  $t_F$  ( $t_H$ ) and  $\sigma_F$  ( $\sigma_H$ ) are the thickness and conductivity of the FMM (HM) layer, respectively.

Note  $\mathbf{T}_{\text{SST}}$  only appears for inhomogeneous magnetization texture with[6, 7]

$$\mathbf{T}_{\text{SST}} = B_J \frac{\partial \mathbf{m}}{\partial x} - \beta B_J \mathbf{m} \times \frac{\partial \mathbf{m}}{\partial x}, \quad (3)$$

where  $B_J = g\mu_B P_F J_e^F/(2eM_s)$ , with  $e, g, \mu_B$  being the absolute value of electron charge, the electron  $g$ -factor and Bohr magneton, respectively.  $P_F$  is the spin polarization of  $\mathbf{J}_e^F$ . The two terms in the right hand side of equation (3) are the so-called adiabatic and non-adiabatic STTs, respectively. They are the continuous counterparts of the Slonczewski[2] and FL STTs in spin valves.  $\beta$  is the dimensionless coefficient describing the relative strength of the nonadiabatic STT and usually of the same order as  $\alpha$ . Note that a negative  $J_e^F$  (thus negative  $B_J$ ) means electrons flow in  $+\mathbf{e}_x$  direction and a positive velocity means the wall propagates along  $+\mathbf{e}_x$  direction. Previous works have verified that in traveling-wave mode STT-driven DWs always move in the direction of electron flow, which is attributed to the existence of nonadiabatic ingredient ( $\beta$ -term).

Generally SOTs have both FL and ADL components. Each component includes the contributions from both SHE and Rashba SOC. In this work we focus on DW dynamics rather than physical sources of SOTs, thus  $\mathbf{T}_{\text{SOT}}$  can be written as

$$\mathbf{T}_{\text{SOT}} = -\gamma H_{\text{FL}} \mathbf{m} \times \mathbf{e}_y - \gamma H_{\text{ADL}} \mathbf{m} \times (\mathbf{m} \times \mathbf{e}_y). \quad (4)$$

Note that both  $H_{\text{FL}}$  and  $H_{\text{ADL}}$  stem from various physical processes and have the unit of magnetic field. Their ratio varies in a wide range for different trilayer systems.

## 2.2. Static wall configuration

In the absence of external charge current, the magnetization texture eventually evolves into some equilibrium state. The ground state is the one with a single domain which is of little interest. Alternatively, the metastable state with a wall separating two magnetic domains is of great importance for both academic and industrial interests. In this subsection, we provide analytical static wall configuration for further usage.

For statics, the magnetization is no longer function of time but only varies with location along  $x$ -axis in 1D-CCM. By dropping a constant  $-k_E \mu_0 M_s^2/2$ , the energy density for PMA systems [see equation (1)] turns to

$$\mathcal{E}[\mathbf{M}] = \frac{1}{2} \mu_0 M_s^2 \sin^2 \theta (k_E + k_H \cos^2 \phi) + J \left[ \left( \frac{d\theta}{dx} \right)^2 + \sin^2 \theta \left( \frac{d\phi}{dx} \right)^2 \right], \quad (5)$$

where  $\theta$  ( $\phi$ ) is the polar (azimuthal) angle of the magnetization vector, as shown in figure 1a. Physically, a static DW should have minimal magnetic energy of the entire

system. For this purpose, first we should have  $d\phi/dx \equiv 0$  to suppress the exchange energy. Second,

$$\phi \equiv \sigma \frac{\pi}{2}, \quad \sigma = \pm 1 \quad (6)$$

will completely eliminate the contribution of hard axis ( $k_H > 0$ ), thus realize a typical Bloch wall combing with the boundary condition (BC)

$$\mathbf{m}(x = \mp\infty) = \pm\eta\mathbf{e}_z, \quad (7)$$

with  $\eta = \pm 1$  coming from the two-fold symmetry of magnetic anisotropy in easy axis. Note  $\sigma$  in equation (6) is the so-called “wall polarity” describing the sign of nonzero  $\langle m_y \rangle$  for a Bloch wall. We then define  $\mathcal{C} \equiv \sigma\eta$  as the “chirality” of Bloch walls.  $\mathcal{C} = +1(-1)$  corresponds to clockwise (anticlockwise) rotation of magnetization when facing to  $+\mathbf{e}_x$ . After these two steps, the total energy density is lowered to

$$\mathcal{E}[\mathbf{M}] = \frac{1}{2}k_E\mu_0M_s^2 \sin^2\theta + J \left( \frac{d\theta}{dx} \right)^2. \quad (8)$$

Then we determine the static  $\theta$ -profile based on the Lagrangian functional  $L = \int \mathcal{L} d^3\mathbf{r}$  with Lagrangian density

$$\mathcal{L} = \frac{\mu_0M_s}{\gamma} \frac{\partial\phi}{\partial t} (1 - \cos\theta) - \mathcal{E}[\mathbf{M}]. \quad (9)$$

The corresponding Euler equation

$$\frac{d}{dx} \left( \frac{\partial\mathcal{L}}{\partial(d\theta/dx)} \right) - \frac{d}{d\theta} \mathcal{L} = 0 \quad (10)$$

together with the static condition  $\partial\phi/\partial t = 0$  lead to

$$\frac{d^2\theta}{dx^2} = \frac{\sin\theta \cos\theta}{(\Delta_0)^2}, \quad \Delta_0 = \sqrt{\frac{2J}{k_E\mu_0M_s^2}}. \quad (11)$$

Its soliton solution is the well-known Walker profile[81]

$$\ln \tan \frac{\theta}{2} = \eta \frac{x - x_0}{\Delta_0}, \quad (12)$$

where  $\eta$  comes from equation (7) and  $x_0$  denotes the DW center position. In summary, equations (6) and (12) provide the complete wall profile which is often referred to as “Bloch(z) wall”. In 1D-CCM, the tilting angle  $\phi$  and DW center  $x_0$  are the two collective coordinates we are concerned.

At last, after the transformation  $\mathcal{U}_y(\pi/2)$ , a Bloch(z) wall in PMA case changes to an in-plane head-to-head (HH,  $\eta = +1$ ) or tail-to-tail (TT,  $\eta = -1$ ) Néel wall in IPMA case with exactly the same analytical profiles as above.

### 2.3. General scalar LLG equations

In the most general case, an external uniform TMF

$$\mathbf{H}_{\text{TMF}} = H_{\perp} \cos \Phi_{\perp} \mathbf{e}_x + H_{\perp} \sin \Phi_{\perp} \mathbf{e}_y \quad (13)$$

is applied across the whole trilayer. By taking into account the conversion between Descartes and spherical coordinate systems, the vectorial LLG equation (2) can be transformed into the following scalar pair

$$\begin{aligned} (\dot{\theta} + \alpha \sin \theta \dot{\phi}) - B_J (\theta' + \beta \sin \theta \phi') &= \gamma \tilde{A}, \\ (\sin \theta \dot{\phi} - \alpha \dot{\theta}) - B_J (\sin \theta \phi' - \beta \theta') &= \gamma \tilde{B}, \end{aligned} \quad (14)$$

with

$$\begin{aligned} \tilde{A} &= A + H_{\text{FL}} \cos \phi + H_{\text{ADL}} \cos \theta \sin \phi, \\ \tilde{B} &= B + H_{\text{ADL}} \cos \phi - H_{\text{FL}} \cos \theta \sin \phi, \end{aligned} \quad (15)$$

and

$$\begin{aligned} A &\equiv k_{\text{H}} M_s \sin \theta \sin \phi \cos \phi - H_{\perp} \sin(\phi - \Phi_{\perp}) + \frac{2J}{\mu_0 M_s \sin \theta} (\phi' \sin^2 \theta)', \\ B &\equiv M_s \sin \theta \cos \theta (k_{\text{E}} + k_{\text{H}} \cos^2 \phi) - H_{\perp} \cos \theta \cos(\phi - \Phi_{\perp}) \\ &\quad - \frac{2J}{\mu_0 M_s} [\theta'' - (\phi')^2 \sin \theta \cos \theta], \end{aligned} \quad (16)$$

where a dot (prime) means  $\partial/\partial t$  ( $\partial/\partial x$ ).

## 3. DW dynamics under SIA/SHE-SOTs

In this section we present analytical explanations of novelties (i) and (ii) in 1D-CCM under the joint action of STT and SIA/SHE-induced SOTs (meanwhile  $H_{\perp} \equiv 0$ ). We will show the different roles of FL and ADL SOTs in modulating DW dynamics.

### 3.1. Brief review of wall dynamics without SOTs

When driven by pure STTs from electric currents ( $H_{\text{FL}} = H_{\text{ADL}} \equiv 0$ ), the static DW profile in equations (6) and (12) can be generalized to [6, 7]

$$\ln \tan \frac{\theta}{2} = \frac{\eta}{\Delta(\phi)} \left[ x - \int_0^t v(\tau) d\tau \right], \quad \phi = \phi(t), \quad (17)$$

where  $\Delta(\phi)$  is the dynamical DW width and  $v(t)$  is the DW velocity. Suppose

$$\Delta(\phi) \equiv \Delta_0 \sqrt{1 + (k_{\text{H}}/k_{\text{E}}) \cos^2 \phi}, \quad (18)$$

then

$$\tilde{A} = k_{\text{H}} M_s \sin \theta \sin \phi \cos \phi, \quad \tilde{B} = 0. \quad (19)$$

Putting back into equation (14), one has

$$\begin{aligned}\frac{v(t)}{\Delta(\phi)} &= -\frac{\eta\gamma}{2(1+\alpha^2)}H_K \sin 2\phi - \frac{1+\alpha\beta}{1+\alpha^2} \frac{B_J}{\Delta(\phi)}, \\ \dot{\phi} &= \frac{\alpha\gamma}{2(1+\alpha^2)}H_K \sin 2\phi + \frac{\alpha-\beta}{1+\alpha^2} \frac{\eta B_J}{\Delta(\phi)},\end{aligned}\tag{20}$$

with  $H_K \equiv k_H M_s$ . By eliminating the “ $\sin 2\phi$ ” term,  $v(t)$  and  $\dot{\phi}$  are directly related as

$$v(t) = -\frac{\eta\Delta(\phi)}{\alpha}\dot{\phi} - \frac{\beta}{\alpha}B_J.\tag{21}$$

The above equations have several deductions: (a) The initial wall velocity reads  $v_{t=0} = -(1+\alpha\beta)B_J/(1+\alpha^2)$  under the joint action of equations (6) and (20). (b) The WB current density

$$J_W \equiv \frac{2eM_s}{g\mu_B P_F} \cdot \frac{\Delta_0\gamma H_W}{|\alpha-\beta|}, \quad H_W \equiv \frac{\alpha H_K}{2}\tag{22}$$

is obtained by setting  $\dot{\phi} = 0$  in equation (20) as well as the constraint  $|\sin 2\phi| \leq 1$ . Here we neglect the breathing effect of dynamical wall width in equation (18) since in most cases one has  $|k_H| \ll |k_E|$ . Obviously when  $\alpha = \beta$ ,  $J_W = +\infty$  meaning DW always falls into the traveling-wave mode. (c) Equation (21) shows that when  $|J_e| < J_W$  the wall propagates along electron-flow direction in a traveling-wave mode with the velocity  $-\beta B_J/\alpha$  and the tilting angle

$$\phi = \sigma \frac{\pi}{2} - \frac{1}{2} \arcsin \left[ \eta \operatorname{sgn}(\beta - \alpha) \frac{J_e^F}{J_W} \right],\tag{23}$$

where “sgn” is the sign function. Interestingly, the wall polarity ( $\sigma$ ) and BC ( $\eta$ ) both have no effect on STT-driven traveling-wave velocity. Therefore, the wall chirality  $\mathcal{C}$  can be either +1 or -1 without any preference due to the two-fold symmetry in  $\mathcal{E}[\mathbf{M}]$ .

### 3.2. Only FL-SOTs appear

We first consider the case in which only the FL-SOT is present, i.e.

$$H_{\text{FL}} \neq 0, \quad H_{\text{ADL}} = 0, \quad H_{\perp} = 0.\tag{24}$$

In 1D-CCM, a trial DW described by equation (17) can always be adopted to perform analytics. Then  $\tilde{A}$  and  $\tilde{B}$  in equation (15) becomes

$$\tilde{A} = H_{\text{FL}} \cos \phi + \frac{H_K}{2} \sin \theta \sin 2\phi, \quad \tilde{B} = -H_{\text{FL}} \cos \theta \sin \phi.\tag{25}$$

Putting back to the scalar LLG equations, and then integrating over the whole strip ( $\int_{-\infty}^{+\infty} \sin \theta dx / \Delta(\phi) \equiv \int_0^\pi d\theta$ ), one has

$$\begin{aligned}\frac{v(t)}{\Delta(\phi)} &= -\frac{\eta\gamma\mathcal{H}(H_K, H_{\text{FL}}, \phi)}{2(1+\alpha^2)} - \frac{1+\alpha\beta}{1+\alpha^2} \frac{B_J}{\Delta(\phi)}, \\ \dot{\phi} &= \frac{\alpha\gamma\mathcal{H}(H_K, H_{\text{FL}}, \phi)}{2(1+\alpha^2)} + \frac{\alpha-\beta}{1+\alpha^2} \frac{\eta B_J}{\Delta(\phi)},\end{aligned}\tag{26}$$



with the functional

$$\mathcal{H}(H_K, H_{FL}, \phi) = (H_K \sin 2\phi + \pi H_{FL} \cos \phi). \quad (27)$$

Obviously, equation (26) shares the same structure with equation (20), except for the substitution of  $H_K \sin 2\phi$  by the functional  $\mathcal{H}(H_K, H_{FL}, \phi)$ , thus leads to the rediscovery of equation (21). *This means the FL-SOT itself can not change the DW mobility (velocity versus current density). However it does suppress the WB thus increase the upper limit of DW velocity in traveling-wave mode.* To see this, in equation (26) one sets  $\dot{\phi} = 0$ , hence

$$\cos \phi \left( 2 \sin \phi + \pi \frac{H_{FL}}{H_K} \right) = \eta \text{sgn}(\beta - \alpha) \frac{J_e^F}{J_W}. \quad (28)$$

If  $\alpha = \beta$ , then  $\phi = \sigma\pi/2$  is always the solution of the above equation (since  $J_W = +\infty$ ). This means DW always behaves as a traveling wave thus no WB occurs. For  $\alpha \neq \beta$ , equation (28) provides different degree of WB suppression depending on the relationship between  $H_{FL}$  and  $J_e^F$  (thus  $J_e$ ).

*3.2.1.  $H_{FL}$  is proportional to  $J_e^F$  (hence  $J_e$ ):* The typical example of this case is that the Rashba effective field  $H_R$  solely contributes to  $H_{FL}$ . In magnetic systems with SIA, the Rashba SOC is proposed to be responsible for the transfer of orbital angular momentum from the crystal lattice to the magnetization system. The resulting Rashba SOT takes effect via an effective Rashba magnetic field[46, 47]

$$\mathbf{H}_R = \lambda (\mathbf{e}_z \times \mathbf{J}_e^F), \quad \lambda \equiv \frac{\alpha_R P_{sd}}{\mu_0 \mu_B M_s}, \quad (29)$$

where  $P_{sd}$  is a parameter depending on the s-d coupling strength and  $\alpha_R$  is the Rashba parameter describing the Rashba SOC strength. The resulting  $\lambda$  is the conversion factor from current density to the Rashba field and is about  $10^{-8} \sim 10^{-9} \text{ T cm}^2/\text{\AA}$ [25, 26].

First we set  $(H_{FL})_W$  as the absolute effective field strength when  $|J_e^F| = J_W$ . For Rashba case, this means  $(H_{FL})_W = \lambda J_W$ . Then by defining

$$a_W \equiv \frac{\pi (H_{FL})_W}{H_K} > 0, \quad (30)$$

equation (28) is rewritten as

$$\frac{J_e^F}{J_W} = \frac{\kappa J_e}{J_W} = \frac{\sin 2\phi}{\eta \text{sgn}(\beta - \alpha) - a_W \cos \phi}, \quad (31)$$

with  $\kappa \equiv (t_F + t_H)\sigma_F/(t_F\sigma_F + t_H\sigma_H)$ . By maximizing the absolute value of its right hand side, we can get the WB threshold  $J_W^{FL}$  of the total current density  $J_e$ . Without losing generality, we set “ $\eta \text{sgn}(\beta - \alpha) \equiv +1$ ”.

If  $a_W > 1$ ,  $J_e^F/J_W \rightarrow \infty$  when  $\cos \phi = \eta \text{sgn}(\beta - \alpha)/a_W$  thus leading to infinite  $J_W^{FL}$ . When  $a_W = 1$ , as  $\phi \rightarrow 0^+$  one has  $J_e^F/J_W \approx 4\phi^{-1}(1 - \phi^2/2) \rightarrow +\infty$ . Hence finite  $J_W^{FL}$  can only exist for  $0 < a_W < 1$ . Therefore, the critical condition “ $a_W = 1$ ” combining equations (22), (29) and (30) lead to “ $\alpha_R^{\text{th}} \propto |\beta/\alpha - 1|$ ” relationship in the threshold

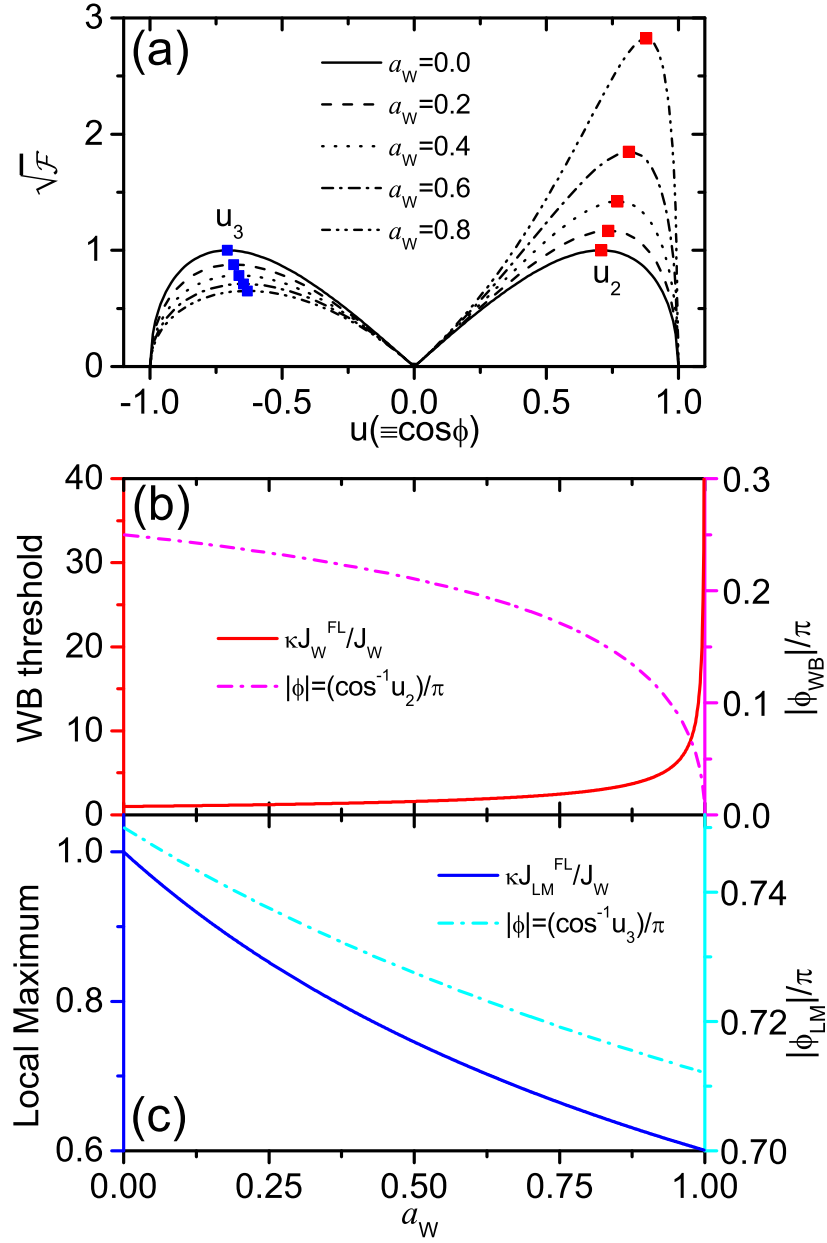


**Figure 2.** (Color online) Extraction of WB and local maximum (LM) from the function  $\sqrt{\mathcal{F}(u)}$  as  $a_W$  varies from 0 to 1: (a) Variation of the function  $\sqrt{\mathcal{F}(u)}$  for  $a_W = 0, 0.2, 0.4, 0.6$  and  $0.8$ . The red (blue) solid squares indicate the normalized WB (LM) position with the horizontal ordinates representing the cosine of corresponding tilting angles, respectively. (b) Normalized WB threshold  $\kappa J_W^{\text{FL}}/J_W$  and the corresponding absolute tilting angle as  $a_W$  increases continuously from 0 to 1. The  $(1 - a_W)^{-1/2}$  divergence of  $\kappa J_W^{\text{FL}}$  can be clearly seen. (c) Normalized LM and the corresponding absolute tilting angle.

above which no WB occurs, thus explicates existing numerical simulations, for example figure 3b in Ref. [70] by Ryu *et al.*

For  $0 < a_W < 1$ , we set  $\cos \phi \equiv u \in [-1, +1]$  and define a new function  $\mathcal{F}(u)$  from (31) as

$$\mathcal{F}(u) \equiv (J_e^F/J_W)^2 = 4u^2(1-u^2)/(1-a_W u)^2. \quad (32)$$

Obviously,  $\mathcal{F}(u)$  is nonnegative. It equals to zero when and only when  $u = 0$  or  $\pm 1$ . To find its extrema, by setting  $\mathcal{F}'(u) = 0$  one obtains four extremal sites:

$$u_{k=1,2,3} = \frac{1}{3a_W} \left[ 2 + 4 \cos \frac{\theta + (2k-3)\pi}{3} \right], \quad u_4 = 0, \quad (33)$$

with  $\theta = \arccos(27a_W^2/16 - 1)$ . Obviously  $u_4$  is the minimum point which can be verified by  $\mathcal{F}''(u_4) > 0$ . When  $a_W \rightarrow 0^+$ , direct calculation yields that  $u_1 \approx 2/a_W - a_W/4 \rightarrow +\infty$  and  $u_{2,3} \approx \pm 1/\sqrt{2} + a_W/8 \rightarrow \pm 1/\sqrt{2}$ , implying that  $u_{2,3}$  are the two maximum points satisfying  $-1 < u_3 < 0 < u_2 < 1$  as shown in figure 2a. Also, it's easy to check  $\mathcal{F}(u_2) > \mathcal{F}(u_3)$ , thus one has,

$$J_W^{\text{FL}} = \kappa^{-1} J_W \sqrt{\mathcal{F}(u_2)}, \quad \phi = \text{sgn}(J_e) \cdot \arccos u_2. \quad (34)$$

To be more intuitive, we plot  $\kappa J_W^{\text{FL}}$  and the corresponding  $|\phi| (= \arccos u_2)$  in figure 2b, which perfectly reproduces existing numerics (for example figure 3a in Ref. [70]). To confirm the WB suppression effect, we then calculate the divergent behavior of  $\kappa J_W^{\text{FL}}$  when  $a_W \rightarrow 1^-$ . Define  $\theta_0 \equiv \arccos(27 \cdot 1^2/16 - 1) = \arccos(11/16)$ , which satisfies  $\cos(\theta_0/3 + \pi/3) = 1/4$ . Suppose  $1 - a_W \equiv \epsilon \rightarrow 0^+$ , it turns out  $u_2 = 1 - \epsilon + o(\epsilon)$  from series expansions. Putting  $u_2$  back into equation (34), after standard series-expansion calculation one gets

$$\kappa J_W^{\text{FL}} \approx \sqrt{2} J_W \cdot (1 - a_W)^{-1/2}, \quad (35)$$

with the corresponding  $\phi$  satisfying

$$|\phi| \approx \sqrt{2} \cdot (1 - a_W)^{1/2}. \quad (36)$$

Equations (35) and (36) perfectly describes the asymptotic behaviors in figure 2b as  $a_W \rightarrow 1^-$ . This confirms the “perfect WB suppression” under appropriate combination of system parameters ( $H_K$ ,  $\kappa$  and  $\lambda$ ). Also, when  $a_W \rightarrow 1^-$  one has  $u_3 \rightarrow (1 - \sqrt{5})/2 \approx -0.618$  and  $\sqrt{\mathcal{F}(u_3)} \rightarrow 2^{-3/2}(\sqrt{5} - 1)^{5/2} \approx 0.6006$ . This is a local maximum (LM) and will be abandoned as  $|J_e| \rightarrow J_W^{\text{FL}}$ . For consistency we also plot the normalized LM and the corresponding absolute tilting angle in figure 2c.

At last, in equation (31) for fixed  $\alpha, \beta$  [thus fixed  $\text{sgn}(\beta - \alpha)$ ] and  $J_e^F$  (hence  $J_e$ ), the “ $\eta \rightarrow -\eta$ ” transformation is equivalent to “ $\phi \rightarrow \pi - \phi$ ” (unchanged  $m_y$  thus wall polarity  $\sigma$ ). This operation will turn the wall chirality  $\mathcal{C}$  to  $-\mathcal{C}$ , hence explains the absence of “chirality selection rule” in numerical simulations with FL-SOT only.

3.2.2.  $H_{\text{FL}}$  is independent of  $J_e^{\text{F}}$  (hence  $J_e$ ): For FL-SOTs coming from other mechanisms, such like BIA or strain,  $H_{\text{FL}}$  would be independent of  $J_e^{\text{F}}$  (hence  $J_e$ ). By setting  $\sin \phi \equiv s \in [-1, +1]$  and  $a \equiv \pi H_{\text{FL}}/H_{\text{K}}$ , another function  $\mathcal{G}(s)$  can be defined from (28) as

$$\mathcal{G}(u) \equiv (J_e^{\text{F}}/J_{\text{W}})^2 = (1 - s^2)(2s + a)^2. \quad (37)$$

$\mathcal{G}(s)$  is also nonnegative and only equals to zero when  $s = \pm 1$  or  $-a/2$ . By requiring  $\mathcal{G}'(s) = 0$ , three extremal sites are obtained

$$s_1 = -\frac{a}{2}, \quad s_2 = \frac{4}{a + \sqrt{a^2 + 32}}, \quad s_3 = -\frac{a + \sqrt{a^2 + 32}}{8}. \quad (38)$$

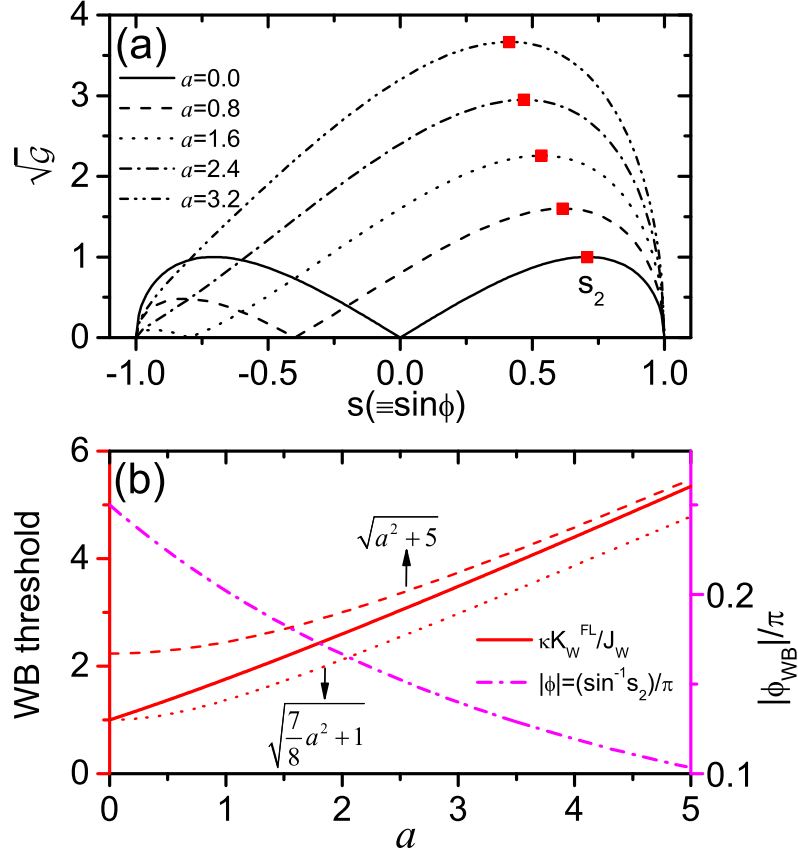


**Figure 3.** (Color online) Extraction of WB threshold from the function  $\sqrt{\mathcal{G}(s)}$  as  $a \equiv \pi H_{\text{FL}}/H_{\text{K}} > 0$ : (a) Variation of the function  $\sqrt{\mathcal{G}(s)}$  for  $a = 0, 0.8, 1.6, 2.4$  and  $3.2$ . Red solid squares indicate the normalized WB position with the horizontal ordinates representing the sine of corresponding tilting angles. (b) Normalized WB threshold  $\kappa K_{\text{W}}^{\text{FL}}/J_{\text{W}}$  and the corresponding absolute tilting angle as  $a$  increases continuously from 1 to 5. The dash (dot) curve represents the upper (lower) boundary of  $\kappa K_{\text{W}}^{\text{FL}}/J_{\text{W}}$ , respectively.

After standard calculus, the function  $\mathcal{G}(s)$  always approaches maximum at  $s = s_2$  when  $a > 0$ , as shown in figure 3a. For  $a < 0$ , similar conclusion holds for  $s = -s_3$ .

Then the corresponding WB threshold [maximum absolute value of the right hand side of equation (28)] reads

$$K_W^{\text{FL}} = \kappa^{-1} J_W \sqrt{\mathcal{G}(s_2)}. \quad (39)$$

Meanwhile, simple calculation yields that  $7a^2/8 + 1 < \mathcal{G}(s_2) < a^2 + 5$ , which confirms the WB suppression at sufficient large  $a$  (i.e.  $H_{\text{FL}}$ ). In figure 3b we plot  $\kappa K_W^{\text{FL}}$  and the corresponding  $\phi$  for  $0 \leq a \leq 5$  when  $\eta \text{sgn}[(\beta - \alpha)J_e] > 0$ . Clearly, the behaviors of WB thresholds in figure 2b and figure 3b are totally different.

In fact, the qualitative role of FL-SOTs has been extensively discussed and now is clear. The driving current ( $J_e^{\text{F}}$ ) pulls the magnetization out of the easy plane, while the demagnetization field ( $H_K$ ) tends to prevent this from happening, leading to the classical Walker limit  $H_W$ . The extra effective SOT field  $H_{\text{FL}}$  in  $\mathbf{e}_y$  axis also helps to prevent the magnetization from leaving the easy plane, thus extending the traveling-wave region of walls. This is the physical origin of WB suppression. Our analytics here provides detailed and solid foundation for the above physical picture: (a) if  $H_{\text{FL}} \propto J_e^{\text{F}}$  (hence  $J_e$ ), both the driving and stabilizing factors tend to grow at the same rate. After appropriately arranging the system parameters ( $H_K$ ,  $\kappa$  and  $\lambda$ ), one has  $a_W \rightarrow 1^-$  thus the WB current is pushed up to infinity (singularity in figure 2b). (b) if  $H_{\text{FL}}$  is independent of  $J_e^{\text{F}}$  (hence  $J_e$ ), then as  $J_e$  increases the WB suppression must have an upper limit, leading to the gentle increment in figure 3b.

### 3.3. Both FL- and ADL-SOTs appear

When both FL- and ADL-SOTs are included, the Walker ansatz in equation (17) is still the start-point of our investigation on DW dynamics. Based on it, one has

$$\begin{aligned} \tilde{A} &= H_{\text{FL}} \cos \phi + H_{\text{ADL}} \cos \theta \sin \phi + \frac{H_K}{2} \sin \theta \sin 2\phi, \\ \tilde{B} &= H_{\text{ADL}} \cos \phi - H_{\text{FL}} \cos \theta \sin \phi. \end{aligned} \quad (40)$$

After putting back into the scalar LLG equations and integrating over the whole strip, it turns out

$$\begin{aligned} \frac{v(t)}{\Delta(\phi)} &= -\frac{\eta\gamma(\mathcal{H} - \alpha\pi H_{\text{ADL}} \cos \phi)}{2(1 + \alpha^2)} - \frac{1 + \alpha\beta}{1 + \alpha^2} \frac{B_J}{\Delta(\phi)}, \\ \dot{\phi} &= \frac{\alpha\gamma(\mathcal{H} + \pi H_{\text{ADL}} \cos \phi / \alpha)}{2(1 + \alpha^2)} + \frac{\alpha - \beta}{1 + \alpha^2} \frac{\eta B_J}{\Delta(\phi)}, \end{aligned} \quad (41)$$

with the same functional  $\mathcal{H}(H_K, H_{\text{FL}}, \phi)$  defined in equation (27). Note that the structure of equation (41) is different from that of equation (20) due to the presence of  $H_{\text{ADL}}$ -terms.

*3.3.1. The WB suppression:* By requiring  $\dot{\phi} = 0$  in equation (41), one gets

$$\cos \phi \left[ 2 \sin \phi + \pi \frac{H_{\text{FL}}}{H_K} \left( 1 + \frac{H_{\text{ADL}}}{\alpha H_{\text{FL}}} \right) \right] = \eta \text{sgn}(\beta - \alpha) \frac{J_e^{\text{F}}}{J_W}, \quad (42)$$

When  $H_{\text{FL}}$  and  $H_{\text{ADL}}$  are both proportional to  $J_e^{\text{F}}$  (generally  $H_{\text{ADL}} \propto J_e^{\text{H}} \propto J_e^{\text{F}}$ ), we set  $(H_{\text{FL}})_{\text{W}}$  and  $(H_{\text{ADL}})_{\text{W}}$  as the absolute effective-field strengths of FL- and ADL-SOTs when  $|J_e^{\text{F}}| = J_{\text{W}}$ . Then after defining

$$b_{\text{W}} \equiv \pi [(H_{\text{FL}})_{\text{W}} + \alpha^{-1} (H_{\text{ADL}})_{\text{W}}] / H_{\text{K}} > 0, \quad (43)$$

equation (42) can be rewritten as

$$\frac{J_e^{\text{F}}}{J_{\text{W}}} = \frac{\kappa J_e}{J_{\text{W}}} = \frac{\sin 2\phi}{\eta \text{sgn}(\beta - \alpha) - b_{\text{W}} \cos \phi}. \quad (44)$$

Then the rest of discussion is the same as in section 3.2.1. When  $H_{\text{FL}}$  and  $H_{\text{ADL}}$  are both independent of  $J_e$ , after setting  $b \equiv \pi (H_{\text{FL}} + \alpha^{-1} H_{\text{ADL}}) / H_{\text{K}}$ , the discussion in section 3.2.2 applies. In both cases, the WB suppression can be explained. At last, we define the increased WB threshold as  $J_{\text{W}}^{\text{FL+ADL}}$  for further usage.

*3.3.2. Mobility change and motion reversal:* After eliminating the  $\mathcal{H}(H_{\text{K}}, H_{\text{FL}}, \phi)$  term in equation (41), one has

$$v(t) = -\frac{\eta \Delta(\phi)}{\alpha} \cdot \dot{\phi} - \frac{\beta}{\alpha} \cdot B_J + \frac{\eta \gamma \pi \Delta(\phi)}{2\alpha} H_{\text{ADL}} \cos \phi. \quad (45)$$

Compared with equation (21), the emergence of  $H_{\text{ADL}}$ -term will lead to the mobility change of DW, or even the motion direction reversal. To see this, suppose  $|J_e| \ll J_{\text{W}}^{\text{FL+ADL}}$  so that the wall is in traveling-wave mode ( $\dot{\phi} = 0$ ) and  $\phi$  is not far away from its static position shown in equation (6). For convenience, we introduce the azimuthal deviation (see figure 1)

$$\psi \equiv \phi - \sigma \frac{\pi}{2}. \quad (46)$$

Since  $|\psi| \ll 1$ , thus  $\cos \phi \approx -\sigma \psi$  and  $\sin 2\phi \approx -2\psi$ . Putting them into equation (42), the azimuthal deviation  $\psi$  can be solved as

$$\psi \approx \frac{(\alpha - \beta) \eta B_J / [\gamma \Delta(\phi) H_{\text{W}}]}{2 + \sigma \pi (H_{\text{FL}} + \alpha^{-1} H_{\text{ADL}}) / H_{\text{K}}}. \quad (47)$$

Substituting all above deductions into the wall velocity in equation (45), after simple algebra one has

$$\frac{v_{\text{ADL}}}{v_{\text{STT}}} = \frac{1 + \frac{\sigma \pi H_{\text{ADL}}}{2H_{\text{K}}} (\zeta + \beta^{-1})}{1 + \frac{\sigma \pi H_{\text{ADL}}}{2H_{\text{K}}} (\zeta + \alpha^{-1})}, \quad v_{\text{STT}} \equiv -\frac{\beta}{\alpha} B_J, \quad (48)$$

with  $\zeta \equiv H_{\text{FL}} / H_{\text{ADL}}$  and can be assumed positive without losing generality. *Obviously, the presence of  $H_{\text{ADL}}$  as well as the condition  $\alpha \neq \beta$  provides us the possibility of changing wall mobility.* Interestingly, the direction of wall motion can even be reversed ( $v_{\text{ADL}} / v_{\text{STT}} < 0$ ) under the following condition

$$\frac{1}{\zeta + \max(\frac{1}{\alpha}, \frac{1}{\beta})} < \frac{(-\sigma) \pi H_{\text{ADL}}}{2H_{\text{K}}} < \frac{1}{\zeta + \min(\frac{1}{\alpha}, \frac{1}{\beta})}. \quad (49)$$

Note that only walls with polarity  $\sigma$  satisfying  $(-\sigma) H_{\text{ADL}} > 0$  can be reversed from electron flow to the charge current direction, which well explains the ‘‘polarity

sensitivity” phenomena in experiments. However,  $\eta$  does not appear in equation (49), revealing the dominant role of the wall polarity rather than chirality. On the other hand, in real materials  $\alpha, \beta \ll 1$ . Therefore the current density under which equation (49) holds can be small enough to ensure the approximation for obtaining equation (47), thus makes the whole deduction coherent.

To numerically check our analytics, in the simplest case we set  $H_{\text{FL}} = 0$  and  $H_{\text{ADL}} \neq 0$  (thus  $\zeta = 0$ ) which corresponds to the case where only ADL-SOT from SHE is considered as in Ref. [71]. In addition, we set  $\alpha = 0.02$ ,  $\beta = 0.01$  meanwhile define  $\sigma\pi H_{\text{ADL}}/(2H_{\text{K}}) \equiv \xi J_e$  and  $B_J \equiv \chi J_e$ . In figure 4 the “ $v_{\text{ADL}}(v_{\text{STT}})$ ” versus “ $\xi J_e$ ” curves are plotted, in which we set  $\chi/\xi \equiv 1$  for simplicity. The black line indicates the linear dependence of  $v_{\text{STT}}$  on  $\xi J_e (= B_J)$ . While the red curve represent the wall velocity when only ADL-SOT is considered. When  $\xi J_e < 0$ , the wall motion begins to be decelerated and then even be reversed to opposition direction when  $\xi J_e = -\beta$ , which is consistent with equation (49). The negatively divergent part of  $v_{\text{ADL}}$  when  $\xi J_e$  decreases to  $-0.02 (= -\alpha)$  reproduces very well the divergent motion-reversal of “ $\theta_{\text{SH}} = +0.1$ ” case in figure 3a of Ref [71]. In addition, the positively divergent part for “ $\xi J_e < -\alpha$ ” indicates the possibility of “velocity boosting” in the original direction (electron flow) by ADL-SOTs. There are few reports in the literature about this and should be worth of more efforts in both simulations and experiments.

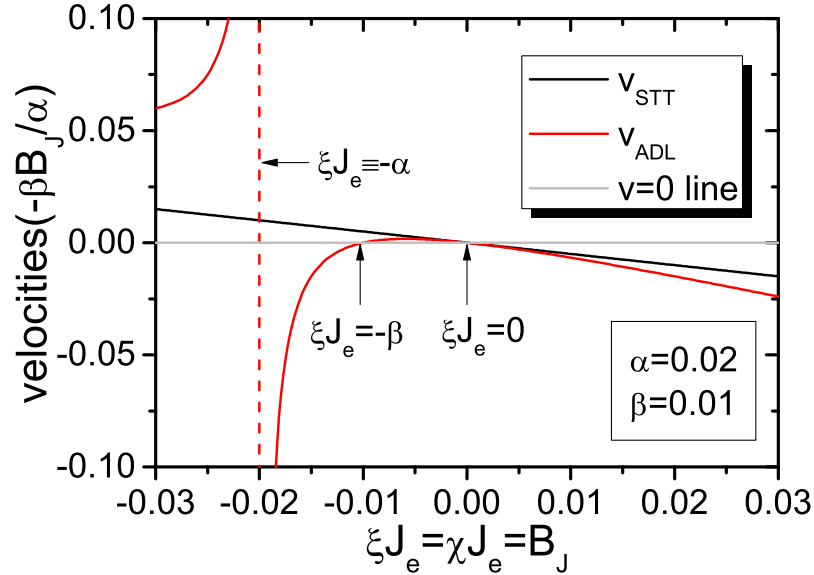


**Figure 4.** (Color online) Mobility change and motion-direction reversal in the presence of ADL-SOT for  $\alpha > \beta$ . Here  $\alpha = 0.02$  and  $\beta = 0.01$  are taken as an example. The solid black line and red curve indicate  $v_{\text{STT}}$  and  $v_{\text{ADL}}$ , respectively. The vertical dash line is the  $\xi J_e \equiv -\alpha$  line where divergence in  $v_{\text{ADL}}$  occurs.

### 3.4. Facts need to be clarified

All analytics in this section are performed based on the trial solution in equation (17). One must bear in mind that it is rigorous only in the absence of any SOTs. When one or both types of SOT are considered (see section 3.2 and section 3.3), in principle equation (17) fails to provide the rigorous wall profile. However, it may serve as a “not-bad” approximation of the actual magnetization texture in magnetic systems with SOC.

Second, as this trial solution can not hold everywhere along  $x$ -direction, to obtain the collective effect we then integrate it over  $x \in (-\infty, +\infty)$  which is transferred to the integration of  $\theta \in (0, \pi)$ . However, when  $J_e$  increases, effective transverse fields from SOTs will pull the magnetization in two faraway domains away from  $z$ -axis. Then the integration of  $x$  over  $(-\infty, +\infty)$  should be converted to that of  $\theta$  over  $(\theta_0, \pi - \theta_0)$ , where  $\theta_0$  is positively correlated with  $J_e$  with some complicated mathematical dependence. For simplicity, we have not considered this  $\theta_0$  in the above subsections. Further investigation on this issue is out of the scope of this work.

In section 3.3.2, by “small quantity analysis” we succeed in explaining the mobility change. In particular, the motion-direction-reversal phenomena as well as the “polarity sensitivity” therein is recovered analytically. In real experiments, the motion-direction-reversal behavior is observed in a relatively wide range of  $J_e$  (thus  $H_{\text{ADL}}$ ). This should not be regarded as a contradiction with equation (49) since it is obtained under the assumption  $|J_e| \ll J_{\text{W}}^{\text{FL}+\text{ADL}}$ . In fact, the necessity of ADL-SOTs for motion-direction-reversal, as well as the polarity sensitivity therein, should be the main focus in this subsection.

At last, by performing  $\mathcal{U}_y(\pi/2)$  introduced in the end of section 2.2, a Bloch wall is transferred into a HH ( $\eta = +1$ ) or TT ( $\eta = -1$ ) Néel wall with unchanged  $m_y$  components in magnetization texture. For Néel walls, the chirality  $\mathcal{C}$  is meaningless but the polarity ( $\sigma$ ) is still valid and unchanged. This explains the feasibility of “polarity sensitivity” of motion-direction-reversal for Néel walls in NiFe FMMs of certain spin-orbit trilayers.

## 4. DW dynamics under general effective TMFs

It is widely accepted that FL-SOTs originating from SIA or SHE have effective TMFs lying in  $y$ -axis. However, for FL-SOTs from other spin-orbit mechanisms, such as BIA or strain, their effective TMFs may lie in  $xy$ -plane with general orientation. Mathematically, they share the same structure with that of external uniform TMFs. Therefore we unify their strength and transverse orientation as  $H_{\perp}$  and  $\Phi_{\perp}$  respectively, and will specify which one is under investigation whenever necessary to avoid possible confusions. The main goal of this section is to investigate whether general effective TMFs alone can lead to mobility change (or even motion-direction-reversal). The coming conclusions also apply to external uniform TMFs.



#### 4.1. Preliminaries

We focus on wall dynamics at low energy-consumption level, thus the traveling-wave mode at low current density is our main concern. Due to the appearance of TMFs, the mismatch between symmetries in different energy terms in transverse direction inevitably induces twisting in  $\phi$ -plane[79]. Thus  $\phi$  is unsuitable to be a collective coordinate any more, leading to the failure of 1D-CCM. Nevertheless, in this region the asymptotic approach[77, 78, 79, 80] is applicable: the dynamical behavior of a DW is viewed as the response of its static profile to external stimuli (here is the injected current), which leads to simultaneous rescaling of current density and velocity (or inverse of time). Meanwhile for external uniform TMF case, the HM layer is assumed unaffected which is a harmless simplification and will not affect our main results since we focus on wall dynamics in FMM layer.

Furthermore, in asymptotic approach we need the static DW profile, which is exactly the zeroth-order solution in asymptotic expansions. Without any transverse fields, the Bloch wall has the rigorous static profile shown in equations (6) and (12). In the presence of a general uniform TMF, recently an approximate static profile has been obtained analytically[79]. For  $0 \leq \sigma\Phi_{\perp} \leq \pi/2$ , the  $\theta$  and  $\phi$  profiles of the static wall are

$$\begin{aligned} \tan \frac{\theta}{2} &= \frac{e^{x_1} + \tan \frac{\theta_{\infty}}{2}}{1 + e^{x_1} \tan \frac{\theta_{\infty}}{2}}, \quad x_1 = \frac{\eta x \cos \theta_{\infty}}{\Delta(\phi_{\infty})}, \quad \theta_{\infty} = \arcsin \left( \frac{H_{\perp}}{H_{\perp}^{\max}} \right), \\ H_{\perp}^{\max} &\equiv M_s \sqrt{k_E^2 \sin^2 \phi_{\infty} + (k_E + k_H)^2 \cos^2 \phi_{\infty}}, \\ \phi_{\infty} &= \arctan \left( \frac{k_E + k_H}{k_E} \tan \Phi_{\perp} \right), \quad \Delta(\phi_{\infty}) = \frac{\Delta_0}{\sqrt{1 + (k_H/k_E) \cos^2 \phi_{\infty}}}, \end{aligned} \quad (50)$$

and

$$\begin{aligned} \frac{|x| - x_2}{\Delta_2} &= F \left( \cos \phi_{\infty}, \arccos \frac{\sqrt{\sin^2 \phi - \sin^2 \phi_{\infty}}}{\cos \phi_{\infty}} \right) \cdot \operatorname{sgn} \left( \sigma \frac{\pi}{2} - \phi \right), \\ x_2 &= \Delta_2 F(\cos \phi_{\infty}), \quad |x| \leq 2x_2, \quad \phi_{\infty} \leq \sigma\phi \leq \pi - \phi_{\infty}, \end{aligned} \quad (51)$$

where  $F(k) \equiv \int_0^{\pi/2} d\zeta / \sqrt{1 - k^2 \sin^2 \zeta}$ ,  $0 < k < 1$  is the complete elliptic integral of the first kind,  $F(k, \psi) \equiv \int_0^{\psi} d\zeta / \sqrt{1 - k^2 \sin^2 \zeta}$ ,  $0 < k < 1$ ,  $0 \leq \psi \leq \pi/2$  is the incomplete elliptic integral of the first kind and  $\Delta_2 = \sqrt{6J/(k_H M_s^2)}$ .

#### 4.2. $H_{\perp}$ is proportional to $J_e$

First we set  $H_{\text{FL}} = H_{\text{ADL}} = 0$  to avoid any contribution of SOTs from SIA or SHE. If  $H_{\perp}$  is induced by charge current, reasonably it is proportional to  $J_e$ . Then, the current density, effective TMF magnitude, and inverse of time are rescaled simultaneously,

$$J_e = \epsilon j_e (B_J = \epsilon b_J), \quad H_{\perp} = \epsilon h_{\perp}, \quad 1/t = \epsilon(1/\tau), \quad (52)$$

where  $\epsilon$  is a dimensionless infinitesimal. The real solution of the LLG equation is expanded as follows,

$$\Omega(x, t) = \Omega_0(x, \tau) + \epsilon \Omega_1(x, \tau) + O(\epsilon^2), \quad \Omega = \theta, \phi. \quad (53)$$

Putting them back into the original LLG equation (14), the solutions to the zeroth-order equation are just equations (6) and (12). At the first order of  $\epsilon$ , with the help of zeroth-order solutions, the differential equation about  $\theta_1$  reads,

$$\begin{aligned}\mathcal{L}\theta_1 &= f_a, \quad \mathcal{L} \equiv \frac{2J}{\mu_0 M_s} \left( -\frac{d^2}{d\xi^2} + \frac{\theta_0'''}{\theta_0'} \right), \\ f_a &\equiv \frac{\eta \sin \theta_0}{\gamma \Delta_0} \left( \alpha \frac{dx_0}{d\tau} + \beta b_J \right) + \sigma h_\perp \cos \theta_0 \sin \Phi_\perp.\end{aligned}\tag{54}$$

Note that  $\mathcal{L}$  is the same 1D self-adjoint Schrödinger operator as given in Refs. [77, 78, 79, 80]. The “Fredholm alternative” demands that  $\theta_0'$  (kernel of  $\mathcal{L}$ ) should be orthogonal to the function “ $f_a$ ” for the existence of solutions to equation (54). This means  $\langle \theta_0', f_a \rangle \equiv \int_{-\infty}^{+\infty} (\theta_0')^* f_a dx = 0$ . Noting that  $\langle \theta_0', \sin \theta_0 \rangle = 2\eta$  and  $\langle \theta_0', \cos \theta_0 \rangle = 0$ , we obtain the wall velocity in traveling-wave mode as

$$V_a = \epsilon dx_0/d\tau = -\beta B_J/\alpha,\tag{55}$$

which reproduces the traveling-wave ( $\dot{\phi} = 0$ ) result in equation (21). This implies in the case of  $H_\perp \propto J_e$ , the effective TMF can not change the wall mobility no matter the transverse angle  $\Phi_\perp$  is.

#### 4.3. $H_\perp$ is independent of $J_e$

Once again, we set  $H_{\text{FL}} = H_{\text{ADL}} = 0$  in advance. If FL-SOTs from BIA or strain induced SOC change very slowly as current density changes, mathematically one can view  $H_\perp$  is finite and independent of  $J_e$ . This assumption also applies to external uniform TMFs which are usually unrelated to  $J_e$ . Then we rescale the current density  $J_e$  and the wall velocity  $V_b$  simultaneously,

$$J_e = \epsilon j_e (B_J = \epsilon b_J), \quad V_b = \epsilon v_b.\tag{56}$$

By defining the traveling coordinate

$$\xi \equiv x - V_b t = x - \epsilon v_b t,\tag{57}$$

the real profiles  $\theta(x, t)$ ,  $\phi(x, t)$  are expanded as

$$\Omega(x, t) = \Omega_0(\xi) + \epsilon \Omega_1(\xi) + O(\epsilon^2), \quad \Omega = \theta, \phi.\tag{58}$$

Substituting equation (58) into LLG equation (14), the solutions to zeroth-order equations are equations (50) and (51). At the first order of  $\epsilon$ , with the help of zeroth-order solutions, the differential equation about  $\theta_1$  and  $\phi_1$  reads,

$$\gamma (\mathcal{L}\theta_1 + \mathcal{M}\phi_1) = f_b,\tag{59}$$

in which  $\mathcal{L}$  still takes the form in equation (54) and

$$\begin{aligned}\mathcal{M} &\equiv \Delta_0^2 k_E M_s \sin 2\theta_0 \left( \phi_0' \frac{d}{d\xi} - \phi_0'' \right), \\ f_b &\equiv v_b (\alpha \theta_0' - \sin \theta_0 \phi_0') + b_J (\beta \theta_0' - \sin \theta_0 \phi_0'),\end{aligned}\tag{60}$$

where a “prime” means  $d/d\xi$ . Note that twisting in  $\phi$ -plane only occurs around the wall center where  $\sin 2\theta_0 \approx 0$ , thus we can neglect the terms proportional to  $\mathcal{M} \approx 0$  [79]. Again,  $\theta'_0$  (kernel of  $\mathcal{L}$ ) should be orthogonal to the function  $f_b$ . Noting that  $\langle \theta'_0, \theta'_0 \rangle = [2 \cos \theta_\infty - (\pi - 2\theta_\infty) \sin \theta_\infty] / \Delta(\phi_\infty)$ , and  $\langle \theta'_0, \sin \theta_0 \phi'_0 \rangle = 0$ , the traveling-wave DW velocity in this situation is,

$$V_b = \epsilon v_b = -\beta B_J / \alpha, \quad (61)$$

which also reproduces equation (21). This result, together with equation (55), reveals that the FL-SOT itself can not change the wall mobility.

#### 4.4. $H_\perp$ is independent of $J_e$ and $H_{\text{ADL}} \propto J_e$

When ADL-SOT in equation (4) is included ( $H_{\text{FL}} = 0$ ,  $H_{\text{ADL}} \propto J_e \neq 0$ ), we perform the same rescaling as in equation (56) plus

$$H_{\text{ADL}} = \epsilon h_{\text{ADL}}. \quad (62)$$

After similar asymptotic-expansion calculations and approximations as in the above subsection, one finally obtains

$$\gamma \mathcal{L} \theta_1 = f_c, \quad f_c = f_b - \gamma h_{\text{ADL}} \cos \phi_\infty. \quad (63)$$

Again, by requiring  $\theta'_0$  being orthogonal to function  $f_c$  one arrives at

$$V_c = -\frac{\beta B_J}{\alpha} + \omega[\theta_0, \phi_0] \frac{\Delta(\phi_\infty)}{\alpha} \gamma H_{\text{ADL}}, \quad (64)$$

in which the nonzero functional

$$\omega[\theta_0, \phi_0] \equiv \frac{\langle \theta'_0, \cos \phi_0 \rangle}{2 \cos \theta_\infty - (\pi - 2\theta_\infty) \sin \theta_\infty} \quad (65)$$

provides the possibility of wall mobility change or even motion-direction reversal as long as nonzero  $H_{\text{ADL}}$  exists.

#### 4.5. Discussions

In this section, we show that to explain experimental novelty (ii) it is necessary to include ADL-SOT. When effective or external TMFs are present, 1D-CCM fails since twisting emerges in  $\phi$ -plane. Therefore asymptotic expansions on LLG equations are adopted to investigate the traveling-wave mode of walls. To obtain the wall velocity in all cases, we have integrated the strip over  $x \in (-\infty, +\infty)$ . The twisting in  $\phi$ -plane has different consequences depending on the terms appearing in the integration kernel. When only  $\theta_0$ -related terms are present, by transferring  $x \in (-\infty, +\infty)$  to  $\theta_0 \in (0, \pi)$  the integration can be easily calculated. In addition, if  $\phi'_0$  appears, the integration turns to be zero due to its odd symmetry. However, if  $\phi_0$ -terms with even symmetry are included (for example,  $\cos \phi_0$ ), generally the integration is hard to be analytically calculated. This is the reason why we did not provide more information on  $\omega[\theta_0, \phi_0]$  in equation (65). It is indeed an interesting issue and should be further investigated in future works.

At last, it should be noted that unlike 1D-CCM, the asymptotic expansion method can not provide WB threshold from its mathematical fundamental. However, it is one of the few ways we have grasped when exploring wall dynamics with mixed symmetry in magnetic energy density.

## 5. Summary

In this work, we analytically investigate the current-induced DW dynamics in HM/FMM/Oxide trilayers with strong SOC's using both 1D-CCM and asymptotic expansion approach. Our results provide clear analytical understandings about the two novelties discovered in experiments and simulations: the FL-SOT itself (no matter what mechanism it stems from) is enough to explain the WB suppression, however to explicate the mobility change or even the motion-direction-reversal, ADL-SOTs are essential. Our analytics should provide insights not only for explaining existing experimental and numerical data (in fact a numbers of simulations have been explained in the main text), but also for the research and development of future DW-propagation-based magnetic nanodevices.

## Acknowledgments

This work is supported by the National Natural Science Foundation of China (Grants Nos. 51671148, 11674251, 51601132 and 11374088). J. Lu also acknowledges the support from the Natural Science Foundation of Hebei Province, China (Grant No. A2014205080), and the Science Foundation for The Excellent Youth Scholars of Educational Commission of Hebei Province, China (Grant No. Y2012027).

## References

- [1] Berger L 1996 Emission of spin waves by a magnetic multilayer traversed by a current *Phys. Rev. B* **54** 9353
- [2] Slonczewski J 1996 Current-driven excitation of magnetic multilayers *J. Magn. Magn. Mater.* **159** L1-L7
- [3] Bazaliy Ya B, Jones B A and Zhang S -C 1998 Modification of the Landau-Lifshitz equation in the presence of a spin-polarized current in colossal- and giant-magnetoresistive materials *Phys. Rev. B* **57** R3213(R)
- [4] Stiles M D and Zangwill A 2002 Anatomy of spin-transfer torque *Phys. Rev. B* **66** 014407
- [5] Tataru G and Kohno H 2004 Theory of current-driven domain wall motion: spin transfer versus momentum transfer *Phys. Rev. Lett.* **92** 086601
- [6] Li Z and Zhang S 2004 Domain-wall dynamics and spin-wave excitations with spin-transfer torques *Phys. Rev. Lett.* **92** 207203
- [7] Zhang S and Li Z 2004 Roles of nonequilibrium conduction electrons on the magnetization dynamics of ferromagnets *Phys. Rev. Lett.* **93** 127204
- [8] Thiaville A, Nakatani Y, Miltat J and Suzuki Y 2005 Micromagnetic understanding of current-driven domain wall motion in patterned nanowires *Europhys. Lett.* **69** 990
- [9] Yan P, Sun Z Z, Schliemann J and Wang X R 2010 Optimal spin current pattern for fast domain wall propagation in nanowires *Europhys. Lett.* **92** 27004

- [10] Sun Z Z, Schliemann J, Yan P and Wang X R 2011 Current-induced domain wall motion with adiabatic and nonadiabatic spin torques in magnetic nanowires *Eur. Phys. J. B* **79** 449
- [11] Grollier J, Boulenc P, Cros V, Hamzić A, Vaurès A, Fert A and Faini G 2003 Switching a spin valve back and forth by current-induced domain wall motion *Appl. Phys. Lett.* **83** 509
- [12] Yamaguchi A, Ono T, Nasu S, Miyake K, Mibu K and Shinjo T 2004 Real-space observation of current-driven domain wall motion in submicron magnetic wires *Phys. Rev. Lett.* **92** 077205
- [13] Kläui M, Jubert P -O, Allenspach R, Bischof A, Bland J A C, Faini G, Rüdiger U, Vaz C A F, Vila L and C. Vouille C 2005 Direct observation of domain-wall configurations transformed by spin currents *Phys. Rev. Lett.* **95** 026601
- [14] Marrows C H 2005 Spin-polarised currents and magnetic domain walls *Adv. Phys.* **54** 585
- [15] Hayashi M, Thomas L, Rettner C, Moriya R, Bazaliy Y B and Parkin S S P 2007 Current driven domain wall velocities exceeding the spin angular momentum transfer rate in Permalloy nanowires *Phys. Rev. Lett.* **98** 037204
- [16] Parkin S S P, Hayashi M and Thomas L 2008 Magnetic domain-wall racetrack memory *Science* **320** 190
- [17] Parkin S S P and Yang S -H 2015 Memory on the racetrack *Nat. Nanotechnol.* **10** 195
- [18] Hayashi M, Thomas L, Moriya R, Rettner C and Parkin S S P 2008 Current-controlled magnetic domain-wall nanowire shift register *Science* **320** 209
- [19] Franken J H, Swagten H J M and Koopmans B 2012 Shift registers based on magnetic domain wall ratchets with perpendicular anisotropy *Nat. Nanotechnol.* **7** 499
- [20] Wang X, Chen Y, Xi H, Li H and Dimitrov D 2009 Spintronic memristor through spin-torque-induced magnetization motion *IEEE Elec. Dev. Lett.* **30** 294
- [21] Münchenberger J, Reiss G and Thomas A 2012 A memristor based on current-induced domain-wall motion in a nanostructured giant magnetoresistance device *J. Appl. Phys.* **111** 07D303
- [22] Khvalkovskiy A V, Zvezdin K A, Gorbunov Ya V, Cros V, Grollier J, Fert A and Zvezdin A K 2009 High domain wall velocities due to spin currents perpendicular to the plane *Phys. Rev. Lett.* **102** 067206
- [23] Boone C T, Katine J A, Carey M, Childress J R, Cheng X and Krivorotov I N 2010 Rapid domain wall motion in Permalloy nanowires excited by a spin-polarized current applied perpendicular to the nanowire *Phys. Rev. Lett.* **104** 097203
- [24] Chanthbouala A, Matsumoto R, Grollier J, Cros V, Anane A, Fert A, Khvalkovskiy A V, Zvezdin K A, Nishimura K, Nagamine Y, Maehara H, Tsunekawa K, Fukushima A and Yuasa S 2011 Vertical-current-induced domain-wall motion in MgO-based magnetic tunnel junctions with low current densities *Nat. Phys.* **7** 626
- [25] Miron I M, Gaudin G, Auffret S, Rodmacq B, Schuhl A, Pizzini S, Vogel J and Gambardella P 2010 Current-driven spin torque induced by the Rashba effect in a ferromagnetic metal layer *Nat. Mater.* **9** 230
- [26] Pi U H, Kim K W, Bae J Y, Lee S C, Cho Y J, Kim K S and Seo S 2010 Tilting of the spin orientation induced by Rashba effect in ferromagnetic metal layer *Appl. Phys. Lett.* **97** 162507
- [27] Liu L, Pai C -F, Li Y, Tseng H W, Ralph D C and Buhrman R A 2012 Spin-torque switching with the giant spin Hall effect of Tantalum *Science* **336** 555
- [28] Liu L, Lee O J, Gudmundsen T J, Ralph D C and Buhrman R A 2012 Current-induced switching of perpendicularly magnetized magnetic layers using spin torque from the spin Hall effect *Phys. Rev. Lett.* **109** 096602
- [29] Garello K, Miron I M, Avci C O, Freimuth F, Mokrousov Y, Blügel S, Auffret S, Boule O, Gaudin G and Gambardella P 2013 Symmetry and magnitude of spinorbit torques in ferromagnetic heterostructures *Nat. Nanotechnol.* **8** 587
- [30] Nguyen M -H, Ralph D C and Buhrman R A 2016 Spin torque study of the spin Hall conductivity and spin diffusion length in Platinum thin films with varying resistivity *Phys. Rev. Lett.* **116** 126601
- [31] Ou Y, Pai C -F, Shi S, Ralph D C and Buhrman R A 2016 Origin of fieldlike spin-orbit torques

- in heavy metal/ferromagnet/oxide thin film heterostructures *Phys. Rev. B* **94** 140414
- [32] Ghosh A, Garello K, Avci C O, Gabureac M and Gambardella P 2017 Interface-Enhanced Spin-Orbit Torques and Current-Induced Magnetization Switching of Pd/Co/AlO<sub>x</sub> Layers *Phys. Rev. Appl.* **7** 014004
  - [33] Moore T A, Miron I M, Gaudin G, Serret G, Auffret S, Rodmacq B, Schuhl A, Pizzini S, Vogel J and Bonfim M 2008 High domain wall velocities induced by current in ultrathin Pt/Co/AlO<sub>x</sub> wires with perpendicular magnetic anisotropy *Appl. Phys. Lett.* **93** 262504
  - [34] Miron I M, Garello K, Gaudin G, Zermatten P -J, Costache M V, Auffret S, Bandiera S, Rodmacq B, Schuhl A and Gambardella P 2011 Perpendicular switching of a single ferromagnetic layer induced by in-plane current injection *Nature* **476** 189
  - [35] Emori S, Bauer U, Ahn S -M, Martinez E and Beach G S D 2013 Current-driven dynamics of chiral ferromagnetic domain walls *Nat. Mater.* **12** 611
  - [36] Lee J -C, Kim K -J, Ryu J, Moon K -W, Yun S -J, Gim G -H, Lee K -S, Shin K -H, Lee H -W and Choe S -B 2011 Universality classes of magnetic domain wall motion *Phys. Rev. Lett.* **107** 067201
  - [37] Miron I M, Moore T, Szabolcs H, Buda-Prejbeanu L D, Auffret S, Rodmacq B, Pizzini S, Vogel J, Bonfim M, Schuhl A and Gaudin G 2011 Fast current-induced domain-wall motion controlled by the Rashba effect *Nat. Mater.* **10** 419
  - [38] Emori S, Bono D C and Beach G S D 2012 Interfacial current-induced torques in Pt/Co/GdOx *Appl. Phys. Lett.* **101** 042405
  - [39] Ryu K -S, Thomas L, Yang S -H and Parkin S S P 2012 Current induced tilting of domain walls in high velocity motion along perpendicularly magnetized micron-sized Co/Ni/Co racetracks *Appl. Phys. Express* **5** 093006
  - [40] Lavrijsen R, Haazen P P J, Murè E, Franken J H, Kohlhepp J T, Swagten H J M and Koopmans B 2012 Asymmetric Pt/Co/Pt-stack induced sign-control of current-induced magnetic domain-wall creep *Appl. Phys. Lett.* **100** 262408
  - [41] Ryu K -S, Thomas L, Yang S -H and Parkin S S P 2013 Chiral spin torque at magnetic domain walls *Nat. Nanotechnol.* **8** 527
  - [42] Linder J and Alidoust M 2013 Asymmetric ferromagnetic resonance, universal Walker breakdown, and counterflow domain wall motion in the presence of multiple spin-orbit torques *Phys. Rev. B* **88** 064420
  - [43] Martinez E, Finocchio G, Torres L and Lopez-Diaz L 2013 The influence of the spin-orbit torques on the current-driven domain wall motion *AIP Advances* **3** 072109
  - [44] Boulle O, Buda-Prejbeanu L D, Jué E, Miron I M and Gaudin G 2014 Current induced domain wall dynamics in the presence of spin orbit torques *J. Appl. Phys.* **115** 17D502
  - [45] Stier M, Creutzburg M and Thorwart M 2014 Rashba-induced chirality switching of domain walls and suppression of the Walker breakdown *Phys. Rev. B* **90** 014433
  - [46] Manchon A and Zhang S 2008 Theory of nonequilibrium intrinsic spin torque in a single nanomagnet *Phys. Rev. B* **78** 212405
  - [47] Manchon A and Zhang S 2009 Theory of spin torque due to spin-orbit coupling *Phys. Rev. B* **79** 094422
  - [48] Matos-Abiague A and Rodríguez-Suárez R L 2009 Spin-orbit coupling mediated spin torque in a single ferromagnetic layer *Phys. Rev. B* **80** 094424
  - [49] Gambardella P and Miron I M 2011 Current-induced spinorbit torques *Philosophical Transactions of the Royal Society A* **369** 3175
  - [50] Haney P M, Lee H -W, Lee K -J, Manchon A and Stiles M D 2013 Current-induced torques and interfacial spin-orbit coupling *Phys. Rev. B* **88** 214417
  - [51] Haney P M, Lee H -W, Lee K -J, Manchon A and Stiles M D 2013 Current induced torques and interfacial spin-orbit coupling: Semiclassical modeling *Phys. Rev. B* **87** 174411
  - [52] Wang X and Manchon A 2012 Diffusive spin dynamics in ferromagnetic thin films with a Rashba interaction *Phys. Rev. Lett.* **108** 117201

- [53] Kim K -W, Seo S -M, Ryu J, Lee K -J and Lee H -W 2012 Magnetization dynamics induced by in-plane currents in ultrathin magnetic nanostructures with Rashba spin-orbit coupling *Phys. Rev. B* **85** 180404
- [54] Pesin D A and MacDonald A H 2012 Quantum kinetic theory of current-induced torques in Rashba ferromagnets *Phys. Rev. B* **86** 014416
- [55] van der Bijl E and Duine R A 2012 Current-induced torques in textured Rashba ferromagnets *Phys. Rev. B* **86** 094406
- [56] Qaiumzadeh A, Duine R A and Titov M 2015 Spin-orbit torques in two-dimensional Rashba ferromagnets *Phys. Rev. B* **92** 014402
- [57] Kurebayashi H, Sinova J, Fang D, Irvine A C, Skinner T D, Wunderlich J, Novk V, Campion R P, Gallagher B L, Vehstedt E K, Zarbo L P, Vyborny K, Ferguson A J and Jungwirth T 2014 An antidamping spinorbit torque originating from the Berry curvature *Nat. Nanotechnol.* **9** 211
- [58] Li H, Gao H, Zârbo L P, Výborný K, Wang X, Garate I, Doğan F, Čejchan A, Sinova J, Jungwirth T and Manchon A 2015 Intraband and interband spin-orbit torques in noncentrosymmetric ferromagnets *Phys. Rev. B* **91** 134402
- [59] Chen W, Sigrist M, Sinova J and Manske D 2015 Minimal model of spin-transfer torque and spin pumping caused by the spin Hall effect *Phys. Rev. Lett.* **115** 217203
- [60] Hirsch J E 1999 Spin Hall effect *Phys. Rev. Lett.* **83** 1834
- [61] Freimuth F, Blügel S and Mokrousov Y 2014 Spin-orbit torques in Co/Pt(111) and Mn/W(001) magnetic bilayers from first principles *Phys. Rev. B* **90** 174423
- [62] Amin V P and Stiles M D 2016 Spin transport at interfaces with spin-orbit coupling: Formalism *Phys. Rev. B* **94** 104419
- [63] Amin V P and Stiles M D 2016 Spin transport at interfaces with spin-orbit coupling: Phenomenology *Phys. Rev. B* **94** 104420
- [64] Ado I A, Tretiakov O A and Titov M 2017 Microscopic theory of spin-orbit torques in two dimensions *Phys. Rev. B* **95** 094401
- [65] Linder J 2013 Chirality-sensitive domain wall motion in spin-orbit coupled ferromagnets *Phys. Rev. B* **87** 054434
- [66] Obata K and Tatara G 2008 Current-induced domain wall motion in Rashba spin-orbit system *Phys. Rev. B* **77** 214429
- [67] He P -B, Zhou Z -D, Wang R -X, Li Z -D, Cai M -Q and Pan A -L 2013 Stability analysis of current-driven domain wall in the presence of spin Hall effect *J. Appl. Phys.* **114** 093912
- [68] Martinez E 2012 Micromagnetic analysis of the Rashba field on current-induced domain wall propagation *J. Appl. Phys.* **111** 033901
- [69] Martinez E 2012 Static Properties and Current-Driven Dynamics of Domain Walls in Perpendicular Magnetocrystalline Anisotropy Nanostrips with Rectangular Cross-Section *Adv. Cond. Matter Phys.* **2012** 954196
- [70] Ryu J, Seo S -M, Lee K -J and Lee H -W 2012 Rashba spinorbit coupling effects on a current-induced domain wall motion *J. Magn. Magn. Mater.* **324** 1449
- [71] Seo S -M, Kim K -W, Ryu J, Lee H -W and Lee K -J 2012 Current-induced motion of a transverse magnetic domain wall in the presence of spin Hall effect *Appl. Phys. Lett.* **101** 022405
- [72] Khvalkovskiy A V, Cros V, Apalkov D, Nikitin V, Krounbi M, Zvezdin K A, Anane A, Grollier J and Fert A 2013 Matching domain-wall configuration and spin-orbit torques for efficient domain-wall motion *Phys. Rev. B* **87** 020402
- [73] Martinez E, Emori S and Beach G S D 2013 Current-driven domain wall motion along high perpendicular anisotropy multilayers: The role of the Rashba field, the spin Hall effect, and the Dzyaloshinskii-Moriya interaction *Appl. Phys. Lett.* **103** 072406
- [74] Martinez E, Emori S, Perez N, Torres L and Beach G S D 2014 Current-driven dynamics of Dzyaloshinskii domain walls in the presence of in-plane fields: Full micromagnetic and one-dimensional analysis *J. Appl. Phys.* **115** 213909
- [75] Gilbert T L 2004 A phenomenological theory of damping in ferromagnetic materials *IEEE Trans.*

*Magn.* **40** 3443

- [76] Matos-Abiague A and Rodríguez-Suárez R L 2009 Spin-orbit coupling mediated spin torque in a single ferromagnetic layer *Phys. Rev. B* **80** 094424
- [77] Goussev A, Lund R G, Robbins J M, Slastikov V and Sonnenberg C 2013 Fast domain-wall propagation in uniaxial nanowires with transverse fields *Phys. Rev. B* **88** 024425
- [78] Goussev A, Lund R G, Robbins J M, Slastikov V and Sonnenberg C 2013 Domain wall motion in magnetic nanowires: an asymptotic approach *Proc. R. Soc. A* **469** 20130308
- [79] Lu J 2016 Statics and field-driven dynamics of transverse domain walls in biaxial nanowires under uniform transverse magnetic fields *Phys. Rev. B* **93** 224406
- [80] Li M, Wang J B and Lu J 2017 General planar transverse domain walls realized by optimized transverse magnetic field pulses in magnetic biaxial nanowires *Sci. Rep.* **7** 43065
- [81] Schryer N L and Walker L R 1974 The motion of  $180^\circ$  domain walls in uniform dc magnetic fields *J. Appl. Phys.* **45** 5406